Astron. Astrophys. 357, 268–282 (2000)

ASTRONOMY AND ASTROPHYSICS

A 5-fluid hydrodynamic approach to model the solar system-interstellar medium interaction

H.J. Fahr, T. Kausch, and H. Scherer

Institut für Astrophysik und Extraterrestrische Forschung der Universität Bonn, Auf dem Hügel 71, 53121 Bonn, Germany

Received 25 October 1999 / Accepted 3 February 2000

Abstract. Since about several decades now it is clearly recognized that the interaction of the solar system with the ambient interstellar medium flow primarily occurs on the basis of a hydrodynamic adaptation of two counterflowing fluids, the solar wind and the interstellar plasmas. The hydrodynamic nature of the interaction unavoidably invokes structures like an inner solar wind termination shock (TS), the heliopause and an outer interstellar bow shock with plasma sheath regions in between. Though the main outlines of this interaction scenario were established long ago, some debates about the location and geometry of these structures still continue up to the present. Fundamentally new aspects of this interaction problem have only quite recently appeared calling for new and more sophisticated calculations. The revisions of the earlier one-fluid interaction concept starts with the consideration of the neutral LISM H-atom gas passing through the solar system. At the occasion of ionizations of this neutral component a medium-energetic plasma component in form of keV-energetic pick-up ions (PUI's) is emerging. This component changes the distant solar wind properties by mass-, momentum-, and energy-loading, as well as by wave generation and lowering the solar wind Mach numbers. Also it has to be taken into account that PUI's serve as seed particles for a high-energetic plasma population with energies between 10 and 100 MeV/nuc called anomalous cosmic rays (ACR's). This latter component together with galactic cosmic rays (GCR's) not only modify the supersonic solar wind by means of their pressure gradients upstream and downstream of the termination shock but also, connected with the ACR shock acceleration process, modulate the shock structure itself. Since all these five fluid components are dynamically coupled, the interaction modes are strongly enriched with respect to what was taken into account in earlier approaches. In the numerical simulations of this paper it is shown how the characteristic features of this complicated 5-fluids interaction scenario look like and which differences occur with respect to the earlier mono- or two-fluid views. As evident the influence of H-atoms and PUI's systematically reduces TS- shock and heliopause locations to smaller scales, whereas ACR's mainly reduce the TS-shock compression ratios. GCR's dependent on their spatial diffusion coefficients more or less blow up the sheath region between the heliopause and the LISM bow shock leaving the rest essentially unchanged.

Key words: hydrodynamics – acceleration of particles – shock waves – Sun: solar wind – inteplanetary medium

1. Introduction

Since the sixties, many different models of the interaction configuration of the solar wind (SW) and the local interstellar medium (LISM) have been presented. The earliest models were analytical approaches (Parker 1963), only taking into account the interaction of the LISM and SW protons or the interaction of SW protons with the LISM magnetic fields. Later models were mostly based on numerical hydrodynamical simulation approaches (Baranov et al. 1976; Baranov & Malama 1993; Steinolfson et al. 1994; Pauls & Zank 1995), demonstrating that earlier assumptions concerning a radially symmetric termination shock with a constant compression ratio is untenable and too much simplifying. Based on numerical models Baranov & Malama (1993), Pauls & Zank (1996), McNutt et al. (1998, 1999) were able to include the interstellar hydrogen population and its interaction with the solar and interstellar protons by means of charge exchange interactions. The first authors followed a kinetic approach treating the neutrals with a Monte Carlo code while the latter authors used a hydrodynamical code and calculated the distribution of the protons on the basis of lowest order velocity moments like density, bulk velocity and scalar temperature.

Furthermore, Izmodenov (1997) has studied in an inconsistent form the dynamical influence of galactic cosmic rays (GCR) using a hydrodynamical fluid code to approach a more complete view of the interaction of LISM and SW media. A more realistic view was later given by Myasnikov et al. (1997) also including back reactions of the GCR pressure on the plasma.

The structure of the termination shock in the presence of pick-up ions, anomalous and galactic cosmic rays was investigated by Donohue & Zank (1993), Chalov & Fahr (1994, 1995, 1997) or Le Roux & Fichtner (1997) in a 1D-model for the upwind direction using a hydrodynamical code for the low-energetic particles, the cold neutral gas model and,

Send offprint requests to: H.J. Fahr (hfahr@astro.uni-bonn.de)

in case of Le Roux & Fichtner (1997) a semi-kinetic, in case of Chalov & Fahr (1997) a hydrodynamical representation for ACR and GCR. The first could thus also give the spectra of these particles at any point on the upwind axis.

Thus many different approaches were exercised to look into the different aspects of the SW-LISM interaction (for a more complete overview see the very comprehensive recent review by Zank (1999) but no model exists up to now investigating all the above mentioned particle populations in a self-consistent manner. This is the aim of the present model approach. We will show the results of a 2D-model treating the consistent interaction of SW- and LISM-protons, pick-up protons, neutral hydrogen atoms, ACR and GCR particles within a self-consistent hydrodynamical 5-fluid approach giving an idea of the spatial distribution of relevant velocity moments of these different particle species in the SW and LISM assuming undisturbed conditions in the distant local interstellar medium.

Not included in the present model are magnetic field influences in a consistent form. Pure magnetohydrodynamic one-fluid models have meanwhile been developed and published by Linde et al. (1998), Ratkiewicz et al. (1998) or Pogorelov & Matsuda (1998, 2000). These, however, do not study influences of neutral atoms, pickup ions, anomalous and galactic cosmic rays. Thus the great synopsis of all field and particle components involved in this interaction scenario will only be given in the near future.

2. Theory of the 5-fluid hydrodynamic interaction

In our approach we make the assumption, that all considered particle populations can be described as hydrodynamical fluids. In all equations derived in the following the index "i" represents one of the five particle species and with the following meaning: i="SP", solar wind – protons; i="PUI", pick up ions; i="ACR", anomalous cosmic rays; i="GCR", galactic cosmic rays; i="IP", (local) interstellar medium – protons; i="H", neutral atoms (e.g. hydrogen).

2.1. Protons, hydrogen atoms and pick-up ions

For the low-energetic particles (i.e. protons (i$\in\{$SP, IP$\}$) and neutral hydrogen (i=H)) we can write the hydrodynamical equations in the following conventional form:

$$\frac{\partial}{\partial t}\rho_i + \boldsymbol{\nabla}\cdot(\rho_i \boldsymbol{u}_i) \;=\; S_{\rho,i} \tag{1}$$

$$\frac{\partial}{\partial t}\rho_i \boldsymbol{u}_i + \boldsymbol{\nabla}\cdot(\rho_i \boldsymbol{u}_i \otimes \boldsymbol{u}_i) + \boldsymbol{\nabla} P_i \;=\; \boldsymbol{S}_{u,i} \tag{2}$$

$$\frac{\partial}{\partial t}E_i + \boldsymbol{\nabla}\cdot(\boldsymbol{u}_i\,(E_i + P_i)) \;=\; S_{E,i} \tag{3}$$

$\rho_i, \boldsymbol{u}_i, P_i$ denoting density, bulk velocity and pressure of the species "i", respectively. The symbol $\otimes$ in Eq. (2) represents the dyadic product. The total energy for these species are given by:

$$E_i = \frac{1}{2}\rho_i |\boldsymbol{u}_i|^2 + \frac{P_i}{\gamma_g - 1} \text{ with } (\gamma_g = \frac{5}{3}). \tag{4}$$

The terms on the right hand side of these equations represent the source terms of protons, PUI's and neutral atoms caused by the mutual interaction with the other species. They will be discussed later in more detail.

Furthermore, we need the PUI density and pressure as they are used as part of the effective plasma pressure and as the seed population for injection into the ACR. Adopting their convection speed to be identical with that of the SW-protons (i.e. $u_{\rm SP}$), we are able to add the following conservation law for the PUI mass flow:

$$\frac{\partial}{\partial t}\rho_{\rm PUI} + \boldsymbol{\nabla}\cdot(\rho_{\rm PUI}\boldsymbol{u}_{\rm SP}) = S_{\rm PUI}. \tag{5}$$

Following the measurements of the Ulysses spacecraft analyzed by Gloeckler et al. (1993), Möbius (1996), Gloeckler & Geiss (1998) the isotropic PUI distribution function can be expressed reasonably well by a rectangular shape in the form:

$$f_{\rm PUI}(\boldsymbol{r}, v) = \begin{cases} \text{const.} & v \le v_{\rm SP}(\boldsymbol{r}) \\ 0 & v > v_{\rm SP}(\boldsymbol{r}) \end{cases} \tag{6}$$

in the solar wind reference frame. This representation for $f_{\rm PUI}$ in Eq. (6) then leads to a PUI pressure of (see Fahr & Fichtner 1995)

$$P_{\rm PUI}(\boldsymbol{r}) = \frac{1}{5}\rho_{\rm PUI} u^2_{\rm SP}(\boldsymbol{r}). \tag{7}$$

which is now introduced in this form into the equations of PUI momentum and energetic flux conservation (Eqs. (1)–(3)) and the ACR seed term (Eq. (13)).

2.2. Galactic and anomalous cosmic rays

The two remaining particle species represent the high energetic ion species, i.e. the ACR and GCR which are negligible by their mass density, however, relevant by their energy density. Their pitch angle-averaged distribution function $f(\boldsymbol{r}, \boldsymbol{p})$ satisfies the transport equation (see Jokipii 1990)

$$\frac{\partial f}{\partial t} + \boldsymbol{u}_{\rm P}\boldsymbol{\nabla} f - \boldsymbol{\nabla}\cdot(\mathsf{K}\,\boldsymbol{\nabla} f) = \frac{1}{3}\,(\boldsymbol{\nabla}\cdot\boldsymbol{u}_{\rm P})\;\boldsymbol{p}\cdot\frac{\partial f}{\partial \boldsymbol{p}} + Q. \tag{8}$$

In this equation guiding center drift motions have been neglected. When assuming a nearly isotropic distribution function, neglecting the mass density of these species with typical energies of 10 to 100 MeV per nucleon, this equation by integration over momentum space leads to the following momentum equation:

$$\frac{\partial E_i}{\partial t} + \boldsymbol{\nabla}\cdot\,(\boldsymbol{u}_{\rm P}E_i) \;+\; (\boldsymbol{v}\boldsymbol{\nabla}\cdot)\,P_i = \boldsymbol{\nabla}\cdot\,(\mathsf{K}\,\boldsymbol{\nabla}E_i) - (\alpha + P_i)\boldsymbol{\nabla}\cdot\,\boldsymbol{u}_{\rm P} \tag{9}$$

with the standard definition

$$E_i = 4\pi\int_{p_1}^{p_2} E(p)p^2 f dp, \quad P_i = \frac{4\pi}{3}\int_{p_1}^{p_2} v p^3 f dp \tag{10}$$

for the energy density and the pressure (i∈{ACR,GCR}). The polytropic relation between E_i and P_i then leads to:

$$E_i = \frac{P_i}{\gamma_i - 1} \tag{11}$$

with the adiabatic index γ_i. This energy-dependent index is held constant within this model for ACR, respectively, GCR because of lack of knowledge of the underlying energetic particle spectra. It is chosen to be $4/3$ for the relativistic GCR ($\bar{E} = 175$MeV/nucleon) and $5/3$ for the non-relativistic ACR ($\bar{E} = 10$MeV/nucleon).

The quantity α describes the local injection rate into the ACR particle-regime from the PUI-regime, i.e. it describes the energy-averaged expression of the production term in Eq. (8). This energy injection rate by means of Fermi-1 acceleration processes is connected with the divergence of the solar wind velocity and operates in a positive sense (i.e. energy supply) in regions of decelerated plasma flows (see also Zank et al. 1993; Chalov & Fahr 1994). According to Zank et al. (1993), α in Eq. (9) can be evaluated with the function f as

$$\alpha = \frac{4\pi}{3}\, E(p_0)\, p_0^3\, f(p_0), \tag{12}$$

where p_0 is the selected threshold separating the PUI from the ACR population. By the same reasons already mentioned before, i.e. non-availability of PUI-distribution function $f_{\rm PUI}(p)$, we are not enabled to follow this formulation strictly but instead we take the approximative representation given by Chalov & Fahr (1994, 1997) and write α in the following parametrized form:

$$\alpha = \alpha' P_{\rm PUI}, \tag{13}$$

where $P_{\rm PUI}$ is the PUI pressure given by Eq. (7) and $\alpha' = \frac{5}{2}$ is a constant injection efficiency defined by the specific plasma properties (see Chalov & Fahr 1997). α' is set to zero for the GCR distribution to respect the fact that no injection occurs into the GCR population.

2.3. The spatial diffusion-coefficient

The elements of the diffusion tensor K in Eq. (9) are generally assumed to be controlled by the local magnetic field $\boldsymbol{B}$. Within the heliospheric termination shock we adopt the Archimedian magnetic field structure derived by Parker (1963). For specifying the spatial diffusion-tensor K in Eq. (9) for application in the inner heliosphere we follow Fichtner et al. (1996) and accordingly take its representation in spherical polar coordinates for the ecliptic (reducing to 2 dimensions; r = radial, θ = azimuthal direction) and due to symmetry conditions with respect to the ecliptic plane one obtains:

$$\mathsf{K} = \begin{pmatrix} K_{rr} & K_{r\theta} \\ K_{\theta r} & K_{\theta\theta} \end{pmatrix} \tag{14}$$

with the elements

$$K_{rr} = \kappa_\parallel \cos^2\psi + \kappa_\perp \sin^2\psi \tag{15}$$

Table 1. $\bar{R}_{\rm ACR}$ is set equal to 0.4 GV because we adopt $\bar{E}_{\rm ACR} = 0.4$ MeV/nucleon (Palmer 1982)

	$\bar{E}/MeV$	$\bar{R}/GV$	$\bar{w}/c$
ACR	10	0.4	0.14
GCR	175	0.6	0.54

$$K_{r\theta} = (\kappa_\parallel - \kappa_\perp)\sin\psi\cos\psi \tag{16}$$

$$K_{\theta r} = \kappa_{r\theta} \tag{17}$$

$$K_{\theta\theta} = \kappa_\parallel \sin^2\psi + \kappa_\perp \cos^2\psi \tag{18}$$

where the tilt angle ψ of the magnetic field with respect to the radial direction is given by Eq. (24), and where $\kappa_\parallel$, $\kappa_\perp$ are the diffusion coefficients parallel and perpendicular to the local Archimedian magnetic field (see Parker 1963). Their momentum dependence can be represented in forms as given by Kota & Jokipii (1993) or Le Roux & Potgieter (1993) leading to the following expressions for momentum-averaged coefficients:

$$\kappa_\parallel = K_0\, \frac{\bar{w}}{c}\, \frac{\bar{R}}{R_0}\, \frac{|B_0|}{B} \;\;,\;\; \kappa_\perp = \beta\kappa_\parallel \tag{19}$$

with the mean values $\bar{w}$ and $\bar{R}$ of the particle velocity and rigidity in gigavolt [GV]. R_0 is taken to be 1 GV, $K_0 = 3.9\,10^{21}$cm^2/s for a reference distance of 1 AU and $\beta = 0.03$ (Fichtner et al. 1996), $\boldsymbol{B}$ is the local magnetic field. The magnitude of the local magnetic field is given by $B = \|\boldsymbol{B}_p\|$ (see next section Eq. (23));

The mean rigidity is defined as

$$\bar{R} = \frac{\bar{p}c}{q} \tag{20}$$

with the mean particle momentum $\bar{p}$ and the particle charge q. The mean energies assumed here and the resulting mean particle velocities and rigidities are listed in Table (1).

In view of the fact that the smallest solar distances considered here are large enough to make the approximation of $\psi \approx 90^\circ$ (Eq. (23)), this results in a great simplification of the diffusion-tensor, i.e. yielding:

$$\mathsf{K} = \begin{pmatrix} \kappa_\perp & 0 \\ 0 & \kappa_\parallel \end{pmatrix}. \tag{21}$$

For the post shock plasma sheath region and for the LISM no accurate information is available about the direction and strength of the local interstellar magnetic field. Thus we are not able to specify components of the interstellar diffusion tensor for ACR ($\kappa_{\rm ACR}$) and GCR ($\kappa_{\rm GCR}$) similar to the form of Eq. (19) but we can set $K_{rr} = K_{\theta\theta} = \kappa$ (i.e scalar diffusion, strong scattering limit) and can extract the ratio of these:

$$\frac{\kappa_{\rm ACR}}{\kappa_{\rm GCR}} = \frac{\bar{w}_{\rm ACR}}{\bar{w}_{\rm GCR}}\, \frac{\bar{R}_{\rm ACR}}{\bar{R}_{\rm GCR}}. \tag{22}$$

Thus we have to specify only one of these coefficients.

2.4. The heliospheric magnetic field

Inside the heliosphere the magnetic field can be approximated by the Parker spiral (Parker 1963) which, in spherical polar coordinates, can be represented by

$$\boldsymbol{B}_P = B_{1AU}\left(\frac{r_{1AU}}{r}\right)^2 (\boldsymbol{e}_r - \boldsymbol{e}_\theta \tan\psi) \tag{23}$$

where $\boldsymbol{e}_r$ and $\boldsymbol{e}_\theta$ are unit vectors in radial and in azimuthal directions, and where

$$\tan\psi = \frac{\Omega\, r}{v_{\rm SW}} \sin\vartheta \tag{24}$$

and where ϑ is the heliospheric co-latitude and $\Omega = 2.9 \cdot 10^{-6}\mathrm{s}^{-1}$ is the angular rotation frequency of the sun.

For a correct consideration of the solar magnetic field, especially outside the termination shock, a full MHD model would be needed which is not yet available and is beyond the scope of this paper. In our two-dimensional model presented here assuming cylindrical symmetry with respect to the LISM-inflow axis also within the heliosphere we can only consider the magnetic field structure in the ecliptic, tacitly assuming that this structure defining radial and azimuthal diffusion processes can be taken as rotationally symmetric with respect to the used symmetry axis, co-aligned with the LISM wind vector. The derived properties in the plasma containing the ecliptic may then be satisfactorily correct, however, in out-of-ecliptic regions the real structures may deviate from our calculations. Additionally, in out-of-ecliptic regions the plasma conditions may also be influenced by ACR and GCR drift motions which were not taken into account in the present approach.

2.5. The interaction of low and high energy particles

The source terms in Eqs. (1)–(3) result from the interaction of protons and neutral hydrogen atoms (P $\leftrightarrow$ H) and in addition from pressure gradients of both middle energetic components (PUI's) and high energetic components (ACR,GCR) and the injection of PUI into the ACR regime (injection rate α Eqs. (12) and (13)). Taking all of this together leads to the following source terms:

$$S_{\rho,\mathrm{P}} = S_\rho^{\mathrm{P}\leftrightarrow\mathrm{H}} \tag{25}$$

$$\boldsymbol{S}_{u,\mathrm{P}} = \boldsymbol{S}_u^{\mathrm{P}\leftrightarrow\mathrm{H}} + \boldsymbol{S}_{u,\mathrm{ACR}} + \boldsymbol{S}_{u,\mathrm{GCR}} + \boldsymbol{\nabla} P_{\mathrm{PUI}} \tag{26}$$

$$S_{E,\mathrm{P}} = S_E^{\mathrm{P}\leftrightarrow\mathrm{H}} + S_{E,\mathrm{ACR}} + S_{E,\mathrm{GCR}} + S_\alpha \tag{27}$$

$$S_{\rho,\mathrm{H}} = S_\rho^{\mathrm{H}\leftrightarrow\mathrm{P}} \tag{28}$$

$$\boldsymbol{S}_{u,\mathrm{H}} = \boldsymbol{S}_u^{\mathrm{H}\leftrightarrow\mathrm{P}} \tag{29}$$

$$S_{E,\mathrm{H}} = S_E^{\mathrm{H}\leftrightarrow\mathrm{P}}. \tag{30}$$

The terms S_{ACR} and S_{GCR} are given by the ACR and GCR pressure gradients:

$$\boldsymbol{S}_{u,\mathrm{ACR}} = -\boldsymbol{\nabla} P_{\mathrm{ACR}} \;,\; S_{E,\mathrm{ACR}} = -\boldsymbol{u}_{\mathrm{P}} \boldsymbol{\nabla} P_{\mathrm{ACR}} \tag{31}$$

$$\boldsymbol{S}_{u,\mathrm{GCR}} = -\boldsymbol{\nabla} P_{\mathrm{GCR}} \;,\; S_{E,\mathrm{GCR}} = -\boldsymbol{u}_{\mathrm{P}} \boldsymbol{\nabla} P_{\mathrm{GCR}} \tag{32}$$

and S_α, S_{ACR} and S_{PUI} in Eq. (27) are given by

$$S_\alpha = \alpha \boldsymbol{\nabla}\cdot\boldsymbol{u}_{\mathrm{P}} \;,\; S_{\mathrm{ACR}} = -S_{\mathrm{PUI}} = -\alpha \boldsymbol{\nabla} \boldsymbol{u}_P. \tag{33}$$

For the proton-hydrogen interaction terms in the LISM we follow McNutt et al. (1998), who gave the most exact representations of the above interaction terms based on the smallest numbers of approximations. In the inner and outer heliosphere we neglect the charge-exchange induced gains of neutral hydrogen atoms since these evidently belong to a new high-velocity particle population (KeV-H-ENA's) (cf. Zank et al. 1996a). As stated by Zank et al. (1996a) this neglection is of minor significance for the heliospheric structure. We use as the relevant charge exchange cross-section the one given by Fite et al. (1962):

$$\sigma_{\mathrm{ex}} = \left[2.1 \cdot 10^{-7} - 9.2 \cdot 10^{-9} \ln(u[\mathrm{cm/s}])\right]^2 [\mathrm{cm}^2]. \tag{34}$$

As result of the description above, one gets the set of coupled differential equations represented in Table 2 describing the interaction of the five particle species: protons (solar wind, interstellar), neutral hydrogen atoms, PUI's, ACR's and GCR's. These coupled differential equations (catalogued in Table 2) have to be solved numerically.

2.6. Photoionisation

Caused by photoionisation an additional loss process of the neutral hydrogen in the solar vicinity occurs. This represents an additional source for the PUI's, in addition to the charge-exchange process. The hydrogen photoionisation rate ν_{PI} near the sun is given by the photoionisation cross section σ_{PI} and the weighted solar EUV-flux F_{EUV}:

$$\nu_{\mathrm{PI}} = \langle \sigma_{\mathrm{PI}} F_{\mathrm{EUV}} \rangle_0 \frac{r_0^2}{r^2} \tag{35}$$

$\langle \sigma_{\mathrm{PI}} F_{\mathrm{EUV}} \rangle_0$ denotes time and frequency averaged product of the cross section and the solar EUV-flux and is assumed to have a constant value of $8\,10^{-8}$ [s^{-1}] at earth's orbit (Fahr 1974). The relative, spectral EUV-flux in Eq. (35) is assumed to be independent of the solar distance, not modified by absorption processes and photoionisation itself. Assuming a solar wind proton density of about 5 [cm^{-3}] and a solar wind speed in the order of $4\,10^7$ [$\mathrm{cm\,s}^{-1}$] photoionisation is a 10–15% effect with respect to the charge exchange and the above approximation of a solar-distance-independent, spectral EUV-flux only plays a minor role.

2.7. Electron impact ionisation

Also by electron impact ionisation a loss of neutral hydrogen atoms occurs, but electron impact ionisation only plays a role in the sheath region downstream of the termination shock, where the electrons are heated up and their thermal velocity (energy) attains the order of the hydrogen ionisation limit (13.6 eV). Due to the low Mach-number flow downstream of the shock ionized hydrogen atoms will not be taken into account as source of PUI's but simply as source of the solar wind protons. The electron impact rate ν_{e} depends on the electron density n_e, the electron velocity v_{e} (energy) with respect to the neutral hydrogen atoms and the impact cross section σ_{e}:

$$\nu_{\mathrm{e}} = \langle \sigma_{\mathrm{e}} v_{\mathrm{e}} \rangle\, n_{\mathrm{e}} \tag{36}$$

Table 2. Resulting hydrodynamical gas equations for protons (index P) and neutral hydrogen (index H), the transport equations for PUI's, ACR's and GCR's and the interaction-terms of protons $\leftrightarrow$ ACR, GCR-interaction

$\frac{\partial}{\partial t}\rho_{\rm P}$	$+$	$\boldsymbol{\nabla}\cdot(\rho_{\rm P}\,\boldsymbol{u}_{\rm P})$	$=$		$S_{\rho,{\rm P}}$	$S_{\rho,{\rm P}}$	$=$	$(\nu_{\rm PI}+\nu_{\rm e})\rho_{\rm H}$
$\frac{\partial}{\partial t}(\rho_{\rm P}\boldsymbol{u}_{\rm P})$	$+\boldsymbol{\nabla}\cdot(\rho_{\rm P}\,\boldsymbol{u}_{\rm P}\,\boldsymbol{u}_{\rm P})+\boldsymbol{\nabla}P_{\rm P}$		$=$		$\boldsymbol{S}_{U,{\rm P}}$	$\boldsymbol{S}_{U,{\rm p}}$	$=$	$-\boldsymbol{\nabla}\,(P_{\rm ACR}+P_{\rm GCR})$
$\frac{\partial}{\partial t}E_{\rm P}$	$+$	${\rm div}\,(\boldsymbol{u}_{\rm P}(E_{\rm P}+P_{\rm P}))$	$=$		$S_{E,{\rm P}}$	$S_{E,{\rm P}}$	$=$	$-\boldsymbol{u}_{\rm P}\cdot\boldsymbol{\nabla}\,(P_{\rm ACR}+P_{\rm GCR})-\alpha\,\boldsymbol{\nabla}\cdot\boldsymbol{u}_{\rm P}$
$\frac{\partial}{\partial t}\rho_{\rm PUI}$	$+$	$\boldsymbol{\nabla}\cdot(\rho_{\rm PUI}\,\boldsymbol{u}_{\rm P})$	$=$		$S_{\rho,{\rm PUI}}$	$S_{\rho,{\rm PUI}}$	$=$	$(\nu_{\rm PI}+\nu_{\rm e}+\nu_{\rm ex})\rho_{\rm H}$
$\frac{\partial}{\partial t}P_{\rm GCR}$	$+$	${\rm div}\,(\boldsymbol{u}_{\rm P}\,P_{\rm GCR})$	$=$	${\rm div}\,(\bar{\kappa}\,\boldsymbol{\nabla}\,P_{\rm GCR})$	$+\;S_{\rm GCR}$	$S_{\rm GCR}$	$=$	$-(\gamma_{\rm GCR}-1)\,P_{\rm GCR}\,\boldsymbol{\nabla}\cdot\boldsymbol{u}_{\rm P}$
$\frac{\partial}{\partial t}P_{\rm ACR}$	$+$	${\rm div}\,(\boldsymbol{u}_{\rm P}\,P_{\rm ACR})$	$=$	${\rm div}\,(\bar{\kappa}\,\boldsymbol{\nabla}\,p_{\rm ACR})$	$+\;S_{\rm ACR}$	$S_{\rm ACR}$	$=$	$-(\gamma_{\rm ACR}-1)\,(P_{\rm ACR}-\alpha)\,\boldsymbol{\nabla}\cdot\boldsymbol{u}_{\rm P}$
$\frac{\partial}{\partial t}\rho_{\rm H}$	$+$	$\boldsymbol{\nabla}\cdot(\rho_{\rm H}\,\boldsymbol{u}_{\rm H})$	$=$		$S_{\rho,{\rm H}}$	$S_{\rho,{\rm H}}$	$=$	$-(\nu_{\rm PI}+\nu_{\rm e})\rho_{\rm H}$
$\frac{\partial}{\partial t}(\rho_{\rm H}\boldsymbol{u}_{\rm H})$	$+\boldsymbol{\nabla}\cdot(\rho_{\rm H}\,\boldsymbol{u}_{\rm H}\,\boldsymbol{u}_{\rm H})+\boldsymbol{\nabla}P_{\rm H}$		$=$		$\boldsymbol{S}_{U,{\rm H}}$	$\boldsymbol{S}_{U,{\rm H}}$	$=$	$-(\nu_{\rm PI}+\nu_{\rm e})\rho_{\rm H}\boldsymbol{u}_{\rm H}-\nu_{\rm ex}\rho_{\rm H}(\boldsymbol{u}_{\rm H}-\boldsymbol{u}_{\rm P})$
$\frac{\partial}{\partial t}E_{\rm H}$	$+$	$\underbrace{{\rm div}\,(\boldsymbol{u}_{\rm H}(E_{\rm H}+P_{\rm H}))}$	$=$	$\underbrace{\qquad\qquad}$	$\underbrace{S_{E,{\rm H}}}$	$S_{E,{\rm H}}$	$=$	$-(\nu_{\rm PI}+\nu_{\rm e})\rho_{\rm H}E_{\rm H}-\nu_{\rm ex}\rho_{\rm H}(E_{\,rmH}-\frac{\rho_{\rm P}}{\rho_{\rm H}}E_{\rm P})$
	$+$	convect. Part		diffus. Part	inter.			

Photoionisation	Electron impact	Charge − exchange
$\nu_{\rm PI}=8\,10^{-8}[{\rm s}^{-1}]\frac{r_0^2}{r^2}$	$\nu_{\rm e}=\sigma_{\rm e}(\langle v_{\rm e,rel.}\rangle)\,\langle v_{\rm e,rel.}\rangle\,n_{\rm e}$	$\nu_{\rm ex}=\sigma_{\rm ex}v_{\rm rel}n_{\rm P}-\sigma_{\rm ex}v_{\rm rel}n_{\rm H}$

which could be approximated by

$$\nu_{\rm e}=\sigma_{\rm e}(\langle v_{\rm e}\rangle)\,\langle v_{\rm e}\rangle\,n_{\rm e} \tag{37}$$

With $n_{\rm e}=n_{\rm p}$ (quasi neutral plasma) the hydrogen-electron impact cross section is given by Kausch & Fahr (1997) with $\sigma_{\rm e}$ in cm^2 and $E_{\rm e}$ in eV:

$$\sigma_{\rm e}=\begin{cases}10^{-17}\frac{a+bE_{\rm e}}{1+cE_{\rm e}+dE_{\rm e}^2} & E_{\rm e}>13.6[{\rm eV}]\\ 0 & E_{\rm e}<13.6[{\rm eV}]\end{cases} \tag{38}$$

Hereby, a,b,c,d are constant and $E_{\rm e}$ the kinetic energy of the electrons relative to the neutral hydrogen atoms with

$$E_{\rm e}=\frac{1}{2}m_{\rm e}v_{\rm e,rel.}^2 \tag{39}$$

Assuming a thermal equilibrium of the plasma ($T_{\rm e}=T_{\rm p}$) the electron velocity relative to the neutral hydrogen atoms is given by

$$v_{\rm e,rel.}\sim\sqrt{\frac{8k_bT_{\rm e}}{\pi m_{\rm e}}}=\sqrt{\frac{m_{\rm e}}{m_{\rm p}}}v_{\rm p,rel.} \tag{40}$$

3. The numerical approach

For the numerical realization of our rotationally symmetric model we introduce a $L\times N$ polar grid in the $(r\,,\theta)$-plane with the sun as its center and the LISM wind vector as symmetry axis. The azimuthal direction $\theta=0^{\rm o}$ points opposite to the LISM wind vector, i.e. to the motion of the solar system relative to the LISM. The coordinates of each cell in this grid are given by its geometrical mid-point (center of volume)

$$\boldsymbol{r}_{l,n}=(r_l,\theta_n) \tag{41}$$

where

$$r_l=R_{\rm min}e^{B\cdot l},\quad B=\frac{1}{L}\ln\left(\frac{\rm R_{max}}{\rm R_{min}}\right),\quad \theta_{\rm n}=\frac{\pi}{\rm N}{\rm n} \tag{42}$$

whereby $R_{\rm min}$ = 10 AU and $R_{\rm max}$ = 3000 AU are chosen. The extension of the cells are defined as

$$\Delta R_l=R_{l+1/2}-R_{l-1/2} \tag{43}$$

$$\Delta\theta_n=\theta_{n+1/2}-\theta_{n-1/2}. \tag{44}$$

Indices $x\pm1/2$ indicate values on the cell boundaries.

In this grid we solve the Eqs. (1)-(3), (5) and (9) by distinguishing between the convective, diffusive, the interaction processes and treating them separately in iteratively and consecutively run procedures.

The convective part of the equations is solved by a Godunov scheme where the spatial resolution is increased to the second order by introducing a piecewise linear distribution of the parameters inside the cells. (For more details see Kausch 1998).

For this procedure of the convective part of Eqs. (1)–(3) and Eq. (9) can be written in the finite-volume formulation as

$$\frac{\boldsymbol{U}^*_{l,n}-\boldsymbol{U}^k_{l,n}}{\Delta t_k}+\frac{\boldsymbol{F}_{l+1/2,n}-\boldsymbol{F}_{l-1/2,n}}{\Delta R_l}+\frac{\boldsymbol{G}_{l,n+1/2}-\boldsymbol{G}_{l,n-1/2}}{r_n\Delta\theta_n}+\boldsymbol{H}_{l,n}=0. \tag{45}$$

Here $\boldsymbol{U}^k_{l,n}$ is the state vector in the cell (l,n) at time-step k, $\boldsymbol{F}$ and $\boldsymbol{G}$ are the fluxes through the cell boundaries. $\boldsymbol{H}$ is a source-term resulting from the used mesh geometry. The resulting intermediate solution for the cell (l,n) is named $\boldsymbol{U}^*$ and is the starting point for calculation of the diffusive part in the cosmic rays equations (ACR and GCR). The corresponding fluxes are calculated by a Roe-type solver (Roe 1981).

The diffusive part is calculated by a fully implicit finite difference scheme. As only the cosmic ray equations have a diffusive part we only have to update E_i^* with i$\in\{$ACR, GCR$\}$. Therefore we get a new intermediate state $\boldsymbol{U}^{**}$ which is equal to $\boldsymbol{U}^*$ except $E^{**}_{\rm ACR}$ and $E^{**}_{\rm GCR}$, which are given as the solution

of (i∈{ACR, GCR})

$$\frac{E^{**}_{i,l,n} - E^{*}_{i,l,n}}{\Delta t_k} = \frac{1}{r_l^2}\frac{1}{\Delta r_l}\Delta_1\left(r^2\kappa_\perp \frac{\Delta_1 E_i^{**}}{\Delta r}\right) + \frac{1}{r_l^2 \sin\theta_n}\frac{1}{\Delta\theta_n}\Delta_2\left(\sin\theta\ \kappa_\parallel \frac{\Delta_2 E_i^{**}}{\Delta\theta}\right) \quad (46)$$

$$\Delta_1 a = a_{l+1/2,n} - a_{l-1/2,n} \quad (47)$$

$$\Delta_2 a = a_{l,n+1/2} - a_{l,n-1/2}. \quad (48)$$

This is the finite-volume formulation of the diffusive part of the cosmic ray equations.

As a last step the source terms have to be included. This is done by the Euler method, whereby

$$\frac{\boldsymbol{U}^{k+1}_{l,n} - \boldsymbol{U}^{**}_{l,n}}{\Delta t_k} = \boldsymbol{S}^{k}_{l,n} \quad (49)$$

the state vector of each cell for time $k+1$ is calculated.

For the considered particle populations we have to apply different boundary conditions for the inner and outer boundary of the grid. The boundaries at $\Theta = 0°$ and $\Theta = 180°$ are on the line of symmetry of this problem (i.e. the LISM apex axis) and by symmetry reasons they are "reflecting" boundaries. The different conditions are as follows:

Protons The inner boundary is an inflow boundary since it is in the region of the unmodulated supersonic solar wind. The parameters at the boundary are given by the physical properties of the SW. The outer boundary is for $\Theta < 90°$ a supersonic LISM inflow boundary, where the protons have the properties of the LISM. For $\Theta > 90°$ a proton flow leaving the integration region is assumed and permanently updated.

Hydrogen atoms The outer boundary is treated like in the case of the protons, but for the inner boundary separately for $\Theta < 90°$ an inflow- and for $\Theta > 90°$ an outflow-boundary have to be applied (first-order extrapolation).

PUI As the PUI strictly convect with the bulk velocity of the protons the inner boundary is an inflow boundary where the boundary values are evaluated by a first-order extrapolation. The outer boundary for $\Theta < 90°$ is in principle again an inflow boundary but due to the fact that the PUI cannot leave the heliosphere, the boundary value is there zero. For $\Theta > 90°$ exists an outflow boundary where the boundary values are given by zero-order extrapolation. This means that we have a vanishing PUI density outside the heliopause.

ACR & GCR Here we apply the condition $\partial p_c/\partial r = 0$ to both, inner and outer, boundaries.

We apply a numerical grid integration code solving the Riemann problem within each grid cell by a Roe-solver of second order. First the conservation equations for the low-energetic species are integrated, then the transport equations for the high-energetic species are solved based on knowledge of the low-energetic plasma properties and finally new source terms are obtained for the conservation equations of the low-energetic plasma species. The whole system is run by successive iterations till finally a consistent solution for all species is obtained. The numerical results give a physically strongly refined picture of the spatial distribution of these different plasma-species demonstrating the relative importance of the interacting species in forming the global interface configuration, i.e. its geometry and dimension.

4. Physics and structure of the particle-modulated inner shock

In earlier numerical simulations of the "solar wind-interstellar medium" interaction the inner shock (termination shock, TS) and the outer shock (bow shock, BS) always have been modeled as a classical hydrodynamic shock described by the well known Rankine-Hugoniot relations (see e.g.Baranov & Malama 1993; Steinolfson et al. 1994; Liewer et al. 1995; Pauls & Zank 1996). Here, however, we intend to also include the dynamics of pick-up ions, anomalous cosmic rays and galactic cosmic rays as we have already described it in the preceding sections. These latter species do, however, also influence the conditions at the shocks by modified effective Mach numbers and modified Rankine-Hugoniot shock relations which have to be properly taken into account in the shock catching procedure and the Riemann problem (see also Ptuskin 1981 or Rice & Zank 1999).

Neutral components of the LISM pass through the inner solar system and at the occasion of ionizations are converted into pick-up ions which are incorporated into the solar wind bulk flow and as a separate ion population are convected to larger solar distances. On the way to the solar wind termination shock these ions suffer acceleration processes by nonlinear interactions with the Alfvénic and magneto-sonic turbulence behaving as wind-entrained, counter-flowing scattering centers (Fermi-II acceleration). These ions load the solar wind with additional mass, momentum and energy, and in the solar wind reference frame constitute a separate KeV-energetic ion species which, contrary to the normal solar wind supersonic proton species, is marginally subsonic. When these ions arrive at the shock they are partly subject there to further acceleration processes (Fermi-I acceleration).

Diffusive acceleration of pick-up ions at the solar wind termination shock is generally seen as source of anomalous cosmic ray particles (Fisk 1976a, 1976b, 1976c; Fisk et al. 1974; Jokipii 1992a, 1992b; Lee et al. 1996; Zank et al. 1996b; Le Roux & Fichtner 1997; Dworsky & Fahr 1999). The shock-generated, anomalous plasma component also represents sufficiently high energy densities to modify the pre-shock solar wind flow by means of its pressure gradient (Jokipii 1990; Fahr et al. 1992; Grzedzielski et al. 1992; Fichtner et al. 1993, 1994; Chalov & Fahr 1994, 1995, 1997). In general in the presence of shock-generated energetic particles a modulated shock wave is formed which essentially consists of a dissipative gas subshock and a smooth precursor upstream formed by energetic particles which are scattered by self-generated upstream wave turbulences. The width of the precursor is determined by the actual value of the diffusion coefficient which is of a fairly uncertain magnitude in the region upstream of the solar wind termination shock. This

coefficient can nevertheless be expected to be sufficiently small for particle energies of between 20 MeV up to about 300 MeV, so that the width of the precursor ($\sim$ 10 AU) will be small compared to the solar distance of the termination shock ($\sim$ 100 AU).

Chalov & Fahr (1994, 1995, 1997) had treated the ACR modulated shock in a parametrized form, prescribing the value χ of the ratio of pick-up ions to solar wind ions at the entrance to the precursor. This ratio, however, cannot be kept as an open parameter for our purposes here, but has to be found in consistency with the other quantities. It has important influences on the nature of the shock and the thermodynamic conditions of the post-shock plasma. The following theoretical approach of the pick-up ion modulated shock is developed on the basis of work presented by Chalov & Fahr (1997). We only mention the basic points of this approach as far as it is applied here.

We consider the pick-up ion modified three-fluid shock as a structure consisting of a shock precursor with decelerated plasma flows and an entropy-generating subshock. At the subshock and also in the precursor region, we consider an energy injection from the 10 KeV-PUI regime into the 10 MeV-ACR regime by means of first-order Fermi processes. The originating high-energy ACR particles are then expected to diffuse relative to the solar wind flow. In this paper we consider the solar wind plasma and the pick-up ions as distinct fluids with different temperatures and densities, but identical bulk velocities u.

Now we are interested in the modified shock relations for a dynamically coupled five-fluid plasma which is considered here. First we assume that the ACR and GCR pressures $P_{\rm c} = P_{\rm ACR} + P_{\rm GCR}$ behave continuous over the subshock transition. Taking $P_{\rm c}$ to be continuous we then obtain the following jump relations at the modified shock:

$$[\mu] = 0, \tag{50}$$

$$[\mu u + P_{\rm g} + P_{\rm PUI}] = 0, \tag{51}$$

$$\mu \left[\frac{u^2}{2} + \frac{\gamma_{\rm g}}{\gamma_{\rm g}-1} \frac{P_{\rm g}+P_{\rm PUI}}{\rho} \right] + [F_{\rm c}] = 0, \tag{52}$$

$$[P_{\rm c}] = 0, \tag{53}$$

$$[F_{\rm c}] = q, \tag{54}$$

with

$$P_{\rm g} + P_{\rm PUI} = P_{\rm P} \tag{55}$$

and where the Poisson brackets [ ] mean differences between quantities on the left side and on the right side of the shock, where μ is the total mass flow normal to the shock, u is the normal component of the plasma bulk velocity, and where the energy injection at the shock, q, is given in the form:

$$q = \lim_{\epsilon \to 0} \int_{-\epsilon}^{+\epsilon} Q(x)\, dx. \tag{56}$$

Here it is assumed that the shock (i.e. the place where the downstream effective Mach number is smaller than 1 i.e. ${M_2^*}^2 = \frac{\mu\, u}{\gamma_{\rm g}(P_{\rm g}+P_{\rm PUI})} \leq 1$ is valid) is found at $x = 0$. Inserting the energy injection rate Q describing ACR energy gains due to the local energy injection into the ACR regime from pick-up ions according to Eq. (13) one obtains:

$$Q(x) = -\alpha P_{\rm PUI} \frac{du}{dx} \tag{57}$$

with $\alpha = \frac{5}{2}$ = const. (see Chalov & Fahr 1997) as the typical ACR injection efficiency. Carrying out the integration in Eq. (56) for step functions in u and P at the shock we then obtain the following result:

$$q = \alpha (u_1 - u_2) \frac{P_{1,\rm PUI} + P_{2,\rm PUI}}{2}, \tag{58}$$

where u_1, u_2, $p_{1,\rm PUI}$ and $p_{2,\rm PUI}$ are the upstream / downstream plasma velocity and pick-up ion pressure, respectively.

In addition to the above mentioned conserved quantities we have to define the quantity $F_{\rm c}$, i.e. the ACR and GCR energy fluxes, which are given by:

$$F_{\rm c} = \sum_c \left(\frac{\gamma_{\rm c}}{\gamma_{\rm c}-1} u P_{\rm c} - \frac{\bar{\kappa}_{\rm c}}{\gamma_{\rm c}-1} \frac{dP_{\rm c}}{dx} \right), \tag{59}$$

where the space coordinate normal to the shock again was denoted by x. The change of $F_{\rm c}$ with respect to x is given by:

$$\frac{dF_{\rm c}}{dx} = \sum_c u_i \frac{dP_{\rm c}}{dx} + Q_{\rm c}(x) \tag{60}$$

Here $\gamma_{\rm c}$ are the polytropic indices of the ACR and GCR species, and $\bar{\kappa}_{\rm c}$ are the respective energy-averaged, scalar diffusion coefficients. Thus with the continuous behaviour of the ACR and GCR pressures at the shock one obtains:

$$[F_{\rm c}] = \alpha (u_1 - u_2) \frac{P_{1,\rm PUI} + P_{2,\rm PUI}}{2}. \tag{61}$$

To close the above system of jump relations we additionally use the fact that the pick-up ion entropy $s_{\rm PUI}$ due to the small pick-up ion pre-shock Mach number remains essentially unchanged at the shock. Then one finally obtains the value z for the shock deceleration $z = \frac{u_2}{u_1}$ by:

$$z = \frac{\gamma_{\rm SP}-1}{\gamma_{\rm SP}+1} \quad \left\{ 1 + \left[\frac{2\gamma_{\rm SP}}{\gamma_{\rm SP}-1} - \alpha(1+\lambda) \right] \cdot \right. \\ \left. \cdot \frac{1}{\gamma_{\rm SP} M_{1,\rm PUI}^2} + \frac{2}{(\gamma_{\rm SP}-1) M_{1,\rm SP}^2} \right\} \tag{62}$$

with $\lambda = \frac{P_{2,\rm PUI}}{P_{1,\rm PUI}}$.

5. Numerical results of the five-fluids interaction model

In the following we want to present results of the above mentioned calculation procedures. At the beginning we shall mention the boundary conditions used in our calculations. The radially symmetric outflow of the unperturbed solar wind flow is described with a bulk velocity of 400 km/s, a proton temperature of 10^5 K and a proton density of 5 cm^{-3} at the orbit of the earth. The LISM conditions are adopted with the following values:

The LISM inflow velocity of both LISM protons and LISM H-atoms amounts to 26 km/s (see Witte et al. 1993), the LISM plasma and gas temperature is assumed to be 8000 K (Bertaux et al. 1985). The unperturbed LISM proton and H-atom densities have both been adopted with $n_{\rm P,LISM} = n_{\rm H,LISM}$ = 0.1 cm^{-3}.

According to Axford & Ip (1986) the LISM GCR pressure can be estimated by:

$$P_{\rm GCR,LISM} = \frac{2}{3}\int_0^{E_1} E\,U(E)dE, \tag{63}$$

where E and $U(E)$ are the energy and the spectral density of GCR particles in the LISM, respectively. With $U(E) = U_0(E_0/E)^{\frac{3}{2}}$ one then obtains:

$$P_{\rm GCR,LISM} = k_{\rm GCR}\sqrt{E_1}\,[{\rm eV/cm^3}], \tag{64}$$

where $k_{\rm GCR}$ is found to have the value $7.2\,10^{-6}$. For an upper energy threshold of E_1 = 300 MeV/nuc one then obtains: $P_{\rm GCR,LISM}$ = 0.2 dyn/cm^2. For higher threshold energies this pressure is correspondingly higher, but what counts for our purposes only is the modulated part of the GCR's which would mean that $E_1 < 1$ GeV/nucleon should be taken which then leads to a value of: $P_{\rm GCR,LISM}$ = 0.28 eV/cm^3; a value which was also selected by Myasnikov et al. (1997).

As already mentioned in the aforegoing sections, the efficiency of a pick-up ion injection into the ACR regime is taken to be proportional to the local pick-up ion pressure with an efficiency factor α'= 5/2 (see Eq. (13)). Within the heliosphere the energy-averaged spatial diffusion coefficients can be found using the corresponding GCR and ACR energy spectra as calculated by le Roux & Fichtner (1997). The ratio of the energy-averaged diffusion coefficients $\kappa_{\rm ACR}/\kappa_{\rm ACR}$ at a solar distance of 5 AU is then found with a value of 0.14.

The charge-exchange induced interactions of H-atoms and ACR's which were considered in the distant heliospheric tail by Czechowski et al. (1995, 1999) has been neglected in this approach here which mainly aims at conditions in the inner heliosphere and the heliosheath. This is a reason why our results presented here for GCR- and ACR-pressures in the distant heliotail should be taken with caution.

5.1. The mono-fluidal test case

First we intend to test our model in the mono-fluid case comparing its results with those of other hydrodynamical models which are already in the literature, e.g. those by Pauls & Zank (1996) or Steinolfson et al. (1994). The latter models are one-fluid hydrodynamic interaction models considering only solar and interstellar protons. For the purpose of such a comparison we thus simply switch off the LISM H-atom inflow leading automatically to a switch-off of the pick-up ion production and the ACR production. In addition we also switch off the GCR influence by setting $\kappa_{\rm GCR}$ = 0. In Figs. 1 a/b/c we have displayed density, radial velocity and temperature of protons in upwind, crosswind and downwind direction.

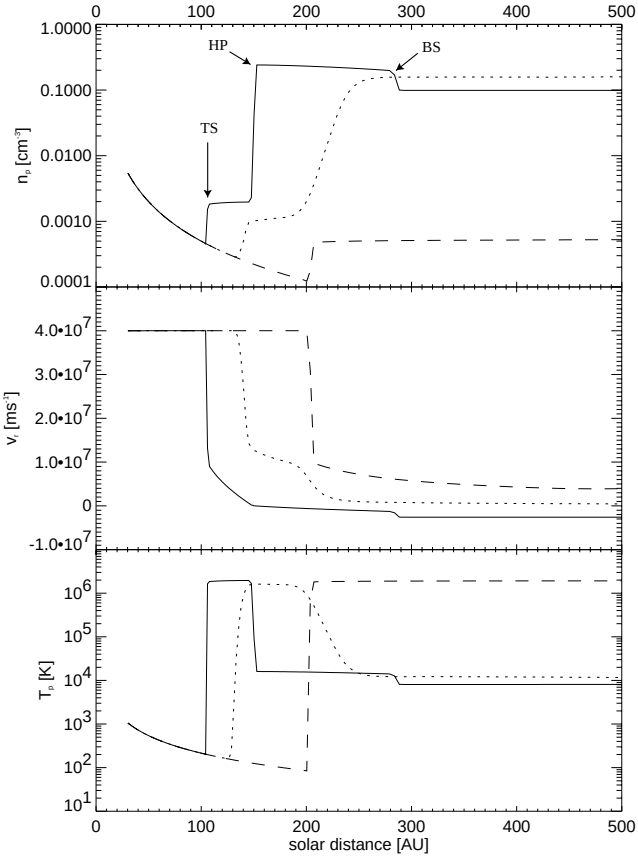

Fig. 1. Resulting density, radial velocity and temperature pattern of the protons in the mono-fluid test case (see text). — Upwind; ··· Crosswind; – – Downwind. Also the position of the solar wind termination shock (TS), of the heliopause (HP) and of the bow-shock (BS) is marked in the upper panel.

One can easily identify the main interaction boundaries like the inner shock (TS), the heliopause (HP) and the outer shock (BS). It is interesting to notice that the inner shock boundary is far from being radially symmetric as assumed in the early approaches by Parker (1963), but is of a bullit-type shape with an upwind shock distance of 105 AU and a downwind shock distance of 205 AU which expresses an upwind/downwind asymmetry of about 0.5. In fact in our calculations the jump conditions at the shock also respect the classical Rankine-Hugoniot conditions yielding a density compression factor of 4 because of the highly supersonic flow upstream of the TS shock.

The heliopause on the upwind axis is located at 150 AU as also found in approaches of the above mentioned authors. The outer shock (BS) has an upwind location at 275 AU and a density compression factor of $s_{\rm BS}$ = 2.05 in our simulation run. The exact Rankine-Hugoniot value is given by:

$$s_{\rm BS} = \frac{(\gamma+1)M^2_{\rm LISM}}{(\gamma-1)M^2_{\rm LISM}+2} = 2.02. \tag{65}$$

The small deviation from the expected value in our simulation is due to the finite spatial resolution of the shock structure. Finally one can state that the results of our simulation run is in accordance with theoretical needs what concerns the jump con-

ditions at the shock and pressure equilibrium at the heliopause. The results displayed in Figs. 1 a/b/c can directly be compared with those presented by Pauls & Zank (1996) and show that for the axially symmetric case they are identical.

5.2. The H-atom and pick-up ion influence

As soon as the LISM H-atom inflow into the heliosphere is switched on, then automatically also pick-up ions are produced by means of charge exchange reactions with the protons. Connected with the production of pick-up ions in the heliosphere is a momentum- and energy-loading of the supersonic solar wind flow. Due to the heating of the solar wind plasma by suprathermal energies of the PUI's the plasma temperature is not anymore adiabatically dropping off with the solar distance. Whereas the vacuum solar wind pressure drops off as $P(r) = P_0(r_0/r)^{2\gamma}$, with γ = 5/3 being the adiabatic index, the pressure of the PUI-heated solar wind drops off roughly with an effective polytrope index of $\gamma_{\rm PUI}$ = 1.44 $\leq$ (5/3).

In connection with the enhanced plasma temperatures at larger distances and lower solar wind velocities due to deceleration by PUI-induced solar wind momentum loading the effective solar wind Mach numbers are drastically reduced with respect to those in the unloaded solar wind. As a main effect of that it turns out that the effective solar wind Mach number at the TS-shock is not any more high. Instead of a strong shock, rather a weak shock hence is established now in upwind direction associated with the preshock Mach number of M_1 = 3.07 and a compression ratio of $s_{\rm TS}$ = 2.96. Due to the decrease of the solar wind kinetic ram pressure the shock has moved inwards to an upwind distance of $R_{\rm TS,up}$ = 81 AU (a downwind distance of $R_{\rm TS,down}$ = 165 AU). Interestingly enough the shock asymmetry factor is nearly unchanged and is again $A = R_{\rm TS,up}/R_{\rm TS,down} = 0.5$ as in the case of the PUI-absence. As well the upwind distance of the outer shock has not changed its position and still is located at $R_{\rm BS,up}$ = 205 AU.

Furthermore, also the heliopause distance has changed and now attains a value of $R_{\rm BS,up}$ = 120 AU. This altogether means that there exists an essential influence of neutral H-atoms on the solar wind plasma flow via charge-exchange induced PUI's as obvious from Figs. 2 a/b/c.

5.3. Neutral H-atoms

The neutral H-atom fluid though not hydrodynamically colliding and interacting with the solar wind plasma flow in a direct sense, like in the case of the LISM proton flow, nevertheless is influenced by the colliding plasma flows by means of charge-exchange interactions. As is shown in Figs. 3 a/b/c the H-atom density thus does not show an outer shock structure at 205 AU but it shows a strong gradual density increase inside of the plasma bow shock. Densities here are increased by a factor of up to 2.5 with respect to the LISM density value. This density increase is caused by the charge-exchange induced deceleration of the H-atom flow due to a soft coupling to the shocked plasma flow. In order to conserve the H-atom flow in this region of deceleration, the H-atom density thus has to be increased accordingly here.

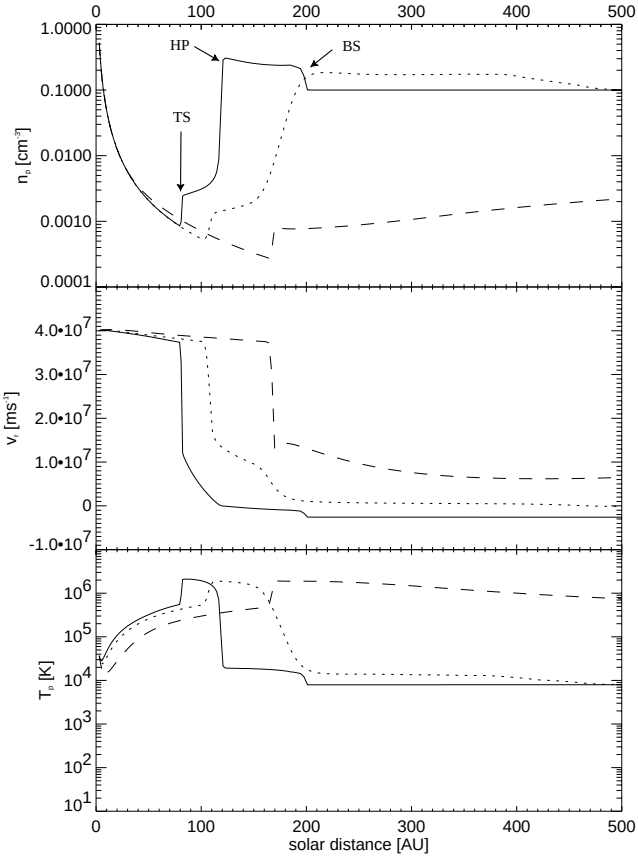

Fig. 2. Density, radial velocity and temperature pattern of the protons when charge-exchange interaction of protons and neutral hydrogen, photoionisation and electron impact ionisation are taken into account. — Upwind; · · · Crosswind; – – Downwind. As in Fig. 1 the position of the solar wind termination shock (TS), of the heliopause (HP) and of the bow shock (BS) is marked in the upper panel.

This phenomenon of the so-called H-atom wall has also been found in similar approaches like those by Baranov & Malama (1993) or Zank et al. (1996a). It is even seen at subsonic LISM inflows as already proven in papers by Osterbart & Fahr (1992), Fahr et al. (1993) and Kausch & Fahr (1997). In this respect it is also very interesting to recognize, that though Baranov & Malama (1993) have used a kinetic treatment for the H-atoms using Monte-Carlo methods they nevertheless found a nearly identical H-atom wall structure as we in our hydrodynamical treatment of the H-atoms both what concerns the absolute density enhancement and the geometrical extent of the wall. Hydrodynamics and kinetics in applications to this problem have also been studied in detail by McNutt et al. (1998, 1999) and led the authors to identical results.

5.4. The pick-up ion distribution

Pick-up ions outside of the heliopause have not been considered in this approach for two reasons: In regions beyond the outer

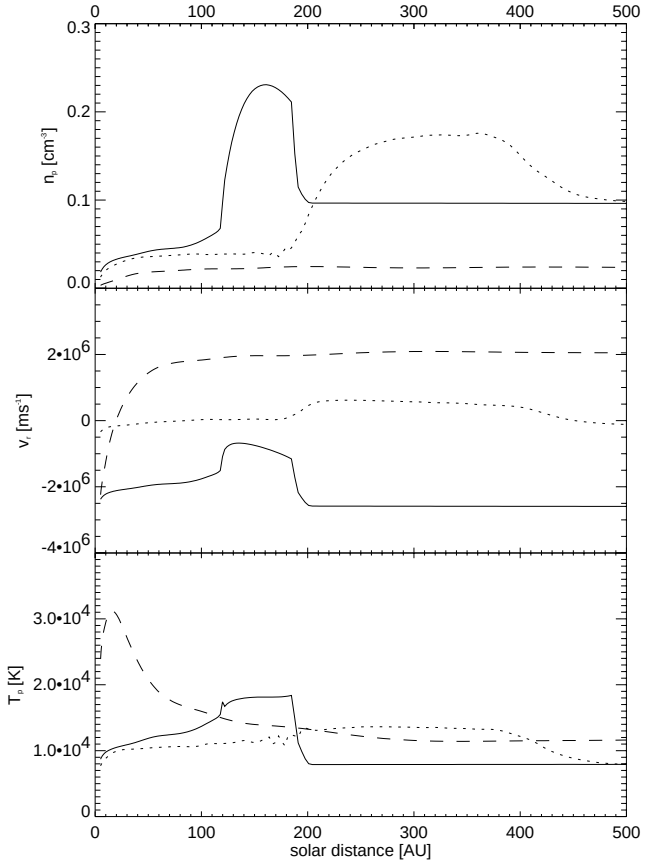

Fig. 3. Density, radial velocity and temperature pattern of the neutral hydrogen when charge-exchange interaction of protons and neutral hydrogen, photoionisation and electron impact ionisation are taken into account. — Upwind; · · · Crosswind; – – Downwind.

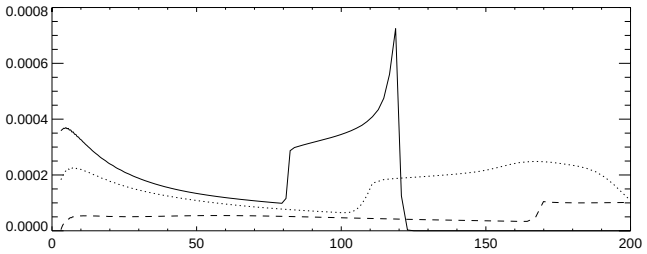

Fig. 4. Radial density pattern of the pick-up ions. — Upwind; · · · Crosswind; – – Downwind.

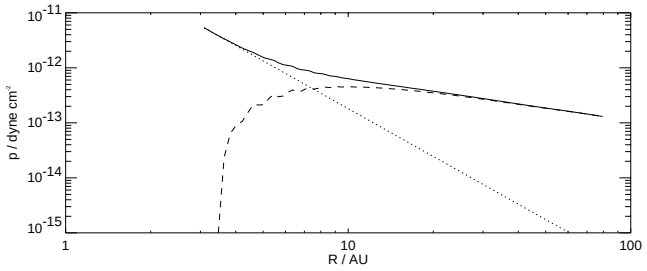

Fig. 5. Radial pressure pattern of the pick-up ions (– –), of the solar wind protons (· · ·) and of the resulting total pressure (—).

shock (BS) we assume LISM equilibrium conditions to prevail. This means that charge exchange reactions between LISM H-atoms and LISM protons in this region beyond the BS shock do not lead to the production of a new species of ions like LISM PUI's. After passage through the BS shock LISM protons exchanging their charge with LISM H-atoms in principle create a new population of ions. In view of the weak shock nature of the BS shock (see Eq. 65) one can, however, tacitly assume that the thermodynamic state of this new ion population is nearly identical with that of the original shocked LISM protons so that no separate consideration of this population is required.

In our approach we do, however, consider pick-up ions in the heliosphere as a separate fluid. These heliospheric pick-up ions were assumed to comove with the solar wind plasma. This is clearly agreed upon by the science community as a fact what concerns pick-up ions in the inner heliosphere (i.e. inside of the TS shock) where the Alfvén velocity is much smaller than the solar wind bulk velocity. It is perhaps less evident in the region downstream of the TS shock where the ratio of the Alfvén velocity over solar wind velocity depends on latitude and longitude of the downstream region. Looking into the appropriate transport equation for PUI's in the downstream region (see Czechowski et al. 1999) one will, however, notice that PUI's as long as they maintain pitch angle-isotropic distributions and undergo negligible spatial diffusion will essentially be convected with the downstream plasma flow.

This then means that PUI's are only seen in the region inside the heliopause as shown in the PUI density diagrams in Fig. 4. The PUI density distribution clearly reflects the TS shock boundary and also shows a strong pile-up of PUI's in the upwind region of the heliospheric sheath where the downstream solar wind plasma flow is decelerated when approaching the heliopause.

In Fig. 5 we also display the PUI pressure along the upwind axis which in regions close to the TS shock is more than two orders of magnitude higher than the solar proton pressure.

5.5. Galactic and anomalous cosmic rays

The important question concerning the role of GCR's concentrates on the actual value of the spatial diffusion coefficient, especially in the region of the LISM. Generally spoken one can state that the galactic cosmic ray fluid is frozen into the LISM plasma flow the more effective, the smaller is the spatial diffusion coefficient.

For very small values of $\kappa_{\rm GCR}$ the GCR's cannot leave the region of their origin, the LISM, and cannot penetrate the heliopause. For very high values of $\kappa_{\rm GCR}$ on the other hand the underlying LISM plasma flow structure does hardly interfere with the spatial GCR pressure distribution. GCR's more or less ignore the plasma structures of the outer heliosphere and the plasma sheath region.

Since unfortunately not very much is known about the adequate value of $\kappa_{\rm GCR}$ we have tested different cases and have used three values for the interstellar diffusion coefficient, namely: $\kappa_{\rm GCR,LISM}$ = 3.9 10^{19} cm^2/s; 3.9 10^{21} cm^2/s; 3.9 10^{23}

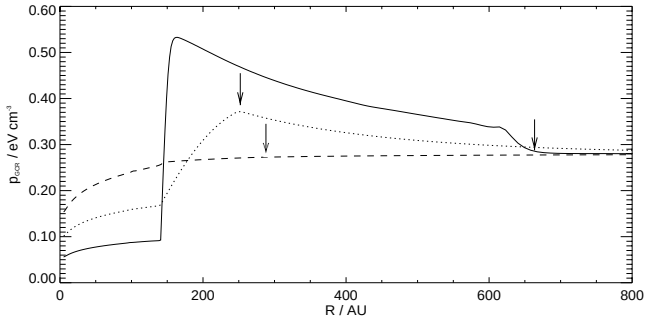

Fig. 6. GCR pressure pattern along the upwind-axis for three different GCR diffusion coefficients $\kappa_{\rm GCR,LISM}$. (—) 3.9 10^{19} cm^2/s; ($\cdots$) 3.9 10^{21} cm^2/s; (– –) 3.9 10^{23} cm^2/s. The position of the bow-shock varys with respect to the different diffusion coefficients and is marked with the arrows.

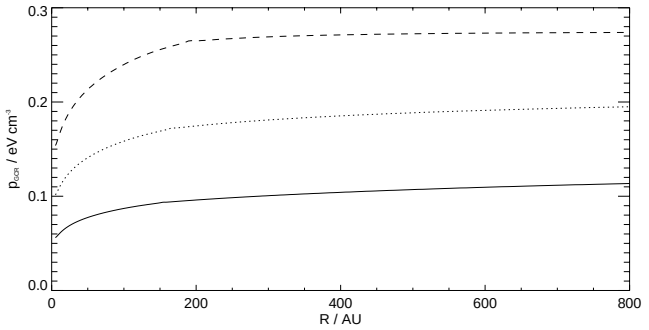

Fig. 7. GCR pressure pattern along the downwind-axis for three different GCR diffusion coefficients $\kappa_{\rm GCR,LISM}$. (—) 3.9 10^{19} cm^2/s; ($\cdots$) 3.9 10^{21} cm^2/s; (– –) 3.9 10^{23} cm^2/s.

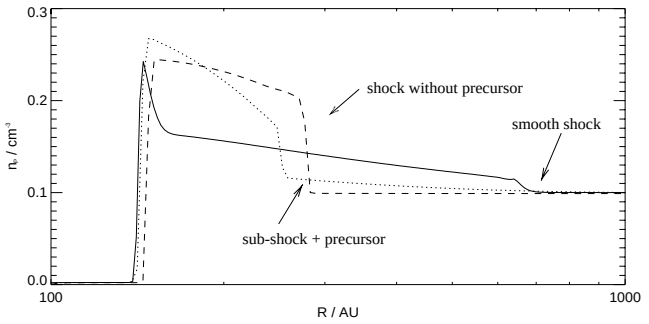

Fig. 8. Region of the bow-shock for three different GCR diffusion coefficients $\kappa_{\rm GCR,LISM}$ (Logarithmic x-axis scale). (—) 3.9 10^{19} cm^2/s; ($\cdots$) 3.9 10^{21} cm^2/s; (– –) 3.9 10^{23} cm^2/s.

cm^2/s. These values include the one used by Myasnikov et al. (1997) and allow a comparison with the results of these authors. As shown in Fig. 6 and in Fig. 7 the three different coefficients $\kappa_{\rm GCR}$ lead to typically different GCR pressure distributions in upwind and downwind direction, especially with very different pressure gradients. In Table 3 we have listed the results for the location of the upwind TS shock, heliopause, and BS shock. Especially in the case of negligible spatial diffusion one can see that due to the freezing-in of the GCR's in the decelerated plasma flow downstream of the BS shock the accumulated GCR pressure in the LISM sheath region strongly blows up this region and places the BS shock to very large distances ($>$ 667 AU).

Table 3. Distance of the termination shock (TS), the heliopause (HP), the bow-shock (BS) and the compression ratios $s_{\rm BS}$ in the upwind direction for different chosen GCR diffusion coefficients. The last line gives the results of the mono-fluid test case when protons are taken into account only (Sect. 5.1)

$\kappa_{G,\rm LISM}\ [cm^2/s]$	$r_{\rm TS}\ [AU]$	$r_{\rm HP}\ [AU]$	$r_{\rm BS}\ [AU]$	$s_{\rm BS}$
$3.9 \cdot 10^{19}$	96	139	>667	1.15
$3.9 \cdot 10^{21}$	98	141	250	1.7
$3.9 \cdot 10^{23}$	101	145	283	2.02
—	105	145	275	2.03

It is also very interesting to pay attention to the nature of the BS shock resulting for different spatial diffusions. This can be studied in more detail in Fig. 8 showing three typical forms of a GCR-modulated shocks. The resulting compression ratios $s_{\rm BS}$ at the BS shock strongly depend on the relative importance of GCR-diffusion over GCR-convection processes as is also recognized by Myasnikov et al. (1997). For strong dominance of diffusion pressure gradients remain small and hardly affect the plasma flow. Hence the compression ratio at the BS shock is mainly determined by the LISM proton Mach number $M_{\rm P,LISM}$. On the other hand, if spatial GCR diffusion is unimportant, then the frozen-in GCR plasma simply represents a high-temperature component incorporated into the LISM plasma. In that case the resulting compression ratio $s_{\rm BS}$ according to Ptuskin (1981) rather than with $M_{\rm P,LISM}$ is connected with the effective Mach number given by:

$$M^{-2}_{\rm eff,LISM} = M^{-2}_{\rm P,LISM} + M^{-2}_{\rm GCR,LISM}, \tag{66}$$

where $M_{\rm GCR,LISM}$ is defined by:

$$M_{\rm GCR,LISM} = \left[\frac{\rho_{\rm P}\ u^2_{\rm P}}{\gamma_{\rm GCR} P_{\rm GCR}}\right]_{\rm LISM}. \tag{67}$$

With the boundary values we have used for the LISM in this paper we obtain the following values for the above mentioned Mach numbers:

$$M_{\rm P,LISM} = 1.75;\ M_{\rm GCR,LISM} = 1.08;\ M_{\rm eff,LISM} = 1.37.$$

Mixed cases for the resulting BS shock are shown in Fig. 8 for the different coefficients $\kappa_{\rm GCR}$ used. For the small value (i.e. $\kappa_{\rm GCR}$ = 3.9 10^{19} cm^2/s, frozen-in GCR plasma) one finds a clearly pronounced BS shock without precursor with an effective compression ratio $s_{\rm BS}$ given by:

$$s_{\rm BS} = \frac{(\gamma+1)M^2_{\rm eff,LISM}}{(\gamma-1)M^2_{\rm eff,LISM}+2} = 1.2. \tag{68}$$

For the case with $\kappa_{\rm GCR}$ = 3.9 10^{21} cm^2/s one finds a modulated BS shock with an interstellar precursor, and for the case with $\kappa_{\rm GCR}$ = 3.9 10^{23} cm^2/s (i.e. decoupled GCR plasma) one obtains a BS shock with a compression ratio given by:

$$s_{\rm BS} = \frac{(\gamma+1)M^2_{\rm eff,LISM}}{(\gamma-1)M^2_{\rm eff,LISM}+2} = 2.02. \tag{69}$$

Included in our interaction model, besides the GCR's, are also the anomalous cosmic rays, the ACR's which have their origin in the region inside the heliopause where due to Fermi-I acceleration processes original PUI seed particles are processed up to energies of the order of 100 MeV/nuc. The injection process from PUI's to ACR's operates all over in the heliosphere where decelerated plasma flows are present, mainly, however, this occurs in the region upstream of the TS shock and at the TS shock itself. According to the mean energies of the ACR's which are lower than those of the GCR's we have calculated their typical spatial diffusion coefficient with $\kappa_{\rm ACR} = 0.138\ \kappa_{\rm GCR}$.

In Fig. 9 we have shown the ACR pressures resulting within our 5-fluids interaction model. As can be seen in this figure ACR's due to the spatial distribution of their sources (i.e. PUI injection rates) are concentrated near the upwind part of the TS shock with relatively strong gradients inwards and outwards from the TS shock. Whereas the ACR pressures are decreasing relatively fast with solar distance on the upwind side, on the downwind side (i.e the heliotail region) our results show a fairly extended ACR pressure distribution extending to distances larger than 250 AU. The absolute calibration of the calculated ACR pressures was carried out such that at an upwind position of 21 AU the measured ACR energy density of 0.0018 eV/cm (see Jokipii 1990) is attained. The downwind results of the ACR pressures presented in Fig. 9 maybe taken with some caution at distances larger than 170 AU because in our calculations no ACR loss processes were taken into consideration while in fact ACR charge exchange reactions with LISM H-atoms start to reduce the ACR pressure at these distances as was already studied in detail by Czechowski et al. (1995).

As mentioned in the first paragraph of Sect. 5 we have scaled the spatial diffusion coefficients of ACR's and GCR's with a constant factor which according to the knowledge one has on the corresponding ACR and GCR particle energy spectra (see LeRoux & Fichtner, 1997) evaluates to $\kappa_{\rm ACR}/\kappa_{\rm GCR}$ = 0.14. Discussing a range of uncertainties in the coefficients $\kappa_{\rm GCR}$ by four orders of magnitude as done in Table 3 of this paper should thus consequently recommend to also consider a similar range in the coefficients $\kappa_{\rm ACR}$. Though we have not yet done this quantitatively here, we nevertheless can easily predict the corresponding consequences for the resulting ACR pressure distributions and their deviations from that given in Fig. 9. Reduction of $\kappa_{\rm ACR}$ with respect to the standard value used in calculations shown in Fig. 9 has the effect of steepening the pressure gradients upstream and downstream of the TS shock while keeping essentially the area below the pressure curve constant due to reasons of conservation of energy deposited in ACR's. Qualitatively one can say that ACR's do show a pile up the closer concentrated around the TS shock surface, the smaller is the spatial diffusion coefficent $\kappa_{\rm ACR}$. A direct observational access to this phenomenon might be opened up by ACR ENA's (i.e. neutral H-atoms with ACR energies) which originate as consequence of ACR's becoming decharged by LISM H-atoms (see Czechowsky et al., 1999, and Fahr & Lay, 2000).

On the contrary, if $\kappa_{\rm ACR}$ is taken to be fairly large with respect to the standard value used in this paper and even to stay at this level also outside the heliopause, then it will turn out that ACR's can easily diffuse away from their source region and enter the trans-heliopause regions, i.e. the LISM side of the interface. In that case the solar system will more or less be surrounded by a radially symmetric halo of ACR's.

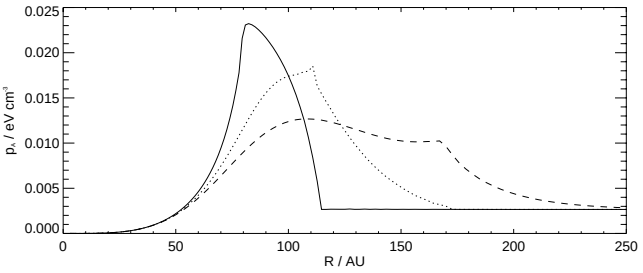

Fig. 9. Radial ACR pressure pattern into three different directions (— upwind; $\cdots$ crosswind; – – downwind). The maxima seen in all three patterns are caused by the injection of the ACR at the termination shock

At the end of this paper we would like to give a synoptic view of the distribution of all interacting fluids considered in this interaction code in the form of colour-coded density or pressure distributions (see Figs. 10–13).

6. Outlook to upcoming modellings

Figs. 10 through 13 give a multicolour vision of the solar wind-interstellar medium interface structure based on a consistent interaction of five different plasma fluids which are dynamically coupled to eachother. Though highly complicated in its synergetics of physical interrelations the picture given here may not approximate the reality acurately enough, since not being complete in some of its genuine aspects. Here we only want to raise a few of them which can direct modellers in the future to improve on the quality of their interface descriptions.

The main flaw in this approach presented here is the fact that we have presented a hydrodynamical simulation only, though a magnetohydrodynamical simulation would be required in fact here. This means, that magnetic fields have not been included in this approach, neither those ones on the solar side nor those on the interstellar side. Consistent magnetic fields, however, are very important in this modelling business mainly because of two reasons:

a) The whole MHD plasma flow structure is strongly influenced by the MHD magnetic fields as is shown in papers by Ratkiewicz et al. (1998), Pogorelov and Matsuda (1998), or Linde et al. (1998).
b) The spatial diffusions and drifts of GCR's and ACR's are effectively controlled both in magnitude and direction by those magnetic fields.

Inclusion of inner and outer magnetic fields will definitely, however, break the symmetry which has been used in the simulation presented in this paper here, meaning that magnetohydrodynamical simulations certainly need a 3-dimensional simulation with much more time-consuming computational efforts. On the other hand, such an extended computational

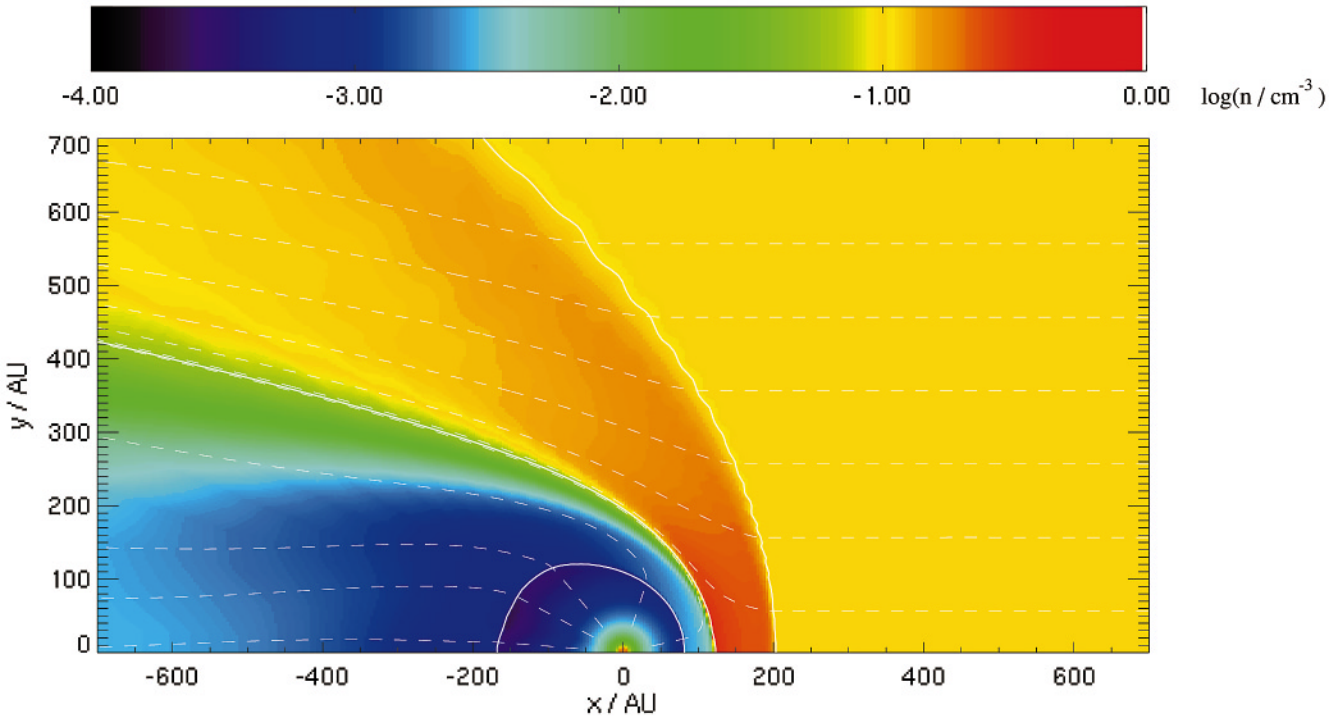

Fig. 10. Contour plot of the resulting proton plasma density pattern ($\log n_P$) and the proton stream lines (white dashed lines) when interactions of protons, neutral hydrogen and pick-up ions are taken into account. Also the positions (white straight lines) of the bow-shock, of the heliopause and of the solar wind termination shock are shown.

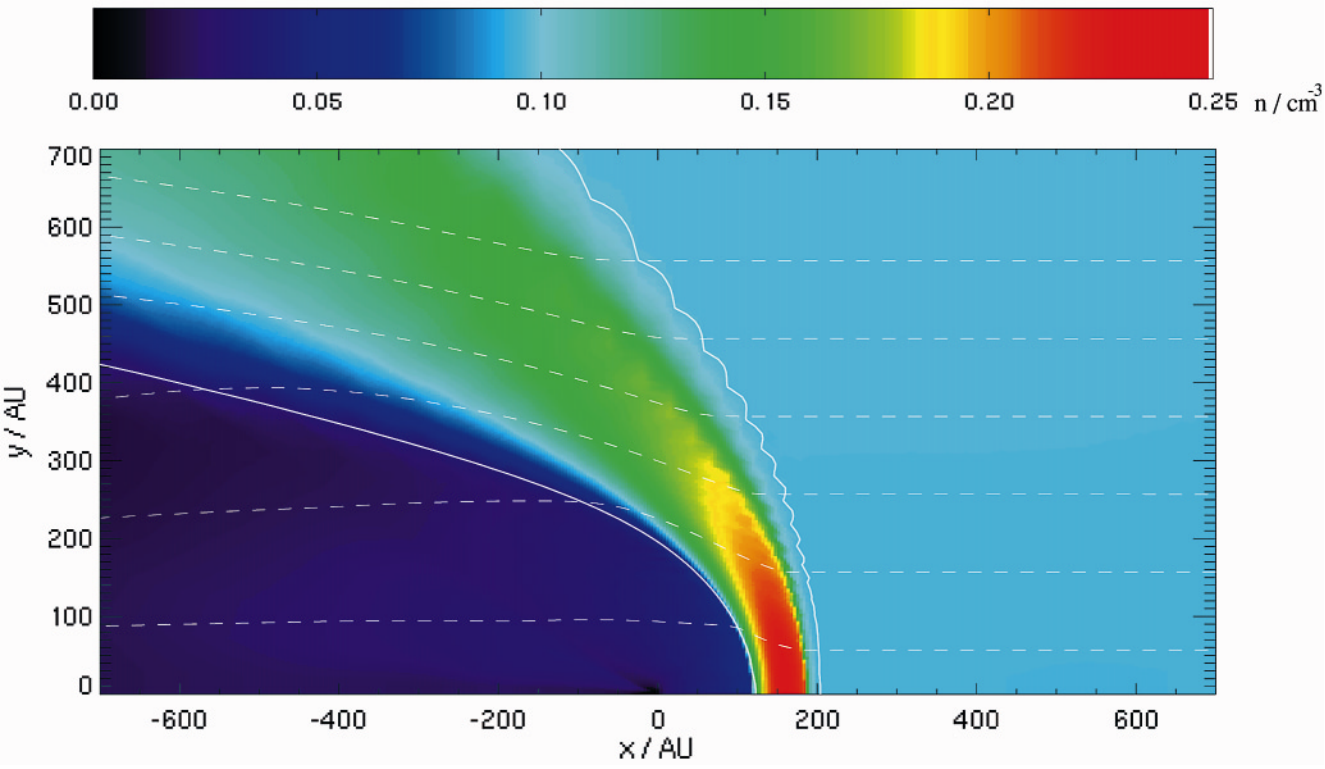

Fig. 11. Contour plot of the neutral hydrogen density pattern and the hydrogen stream lines (white dashed lines) when interactions of protons, neutral hydrogen and pick-up ions are taken into account. For identifying the interface structure (see Fig. 10), also the position of the proton plasmas bow-shock and of the position of the heliopause are shown (white straight lines).

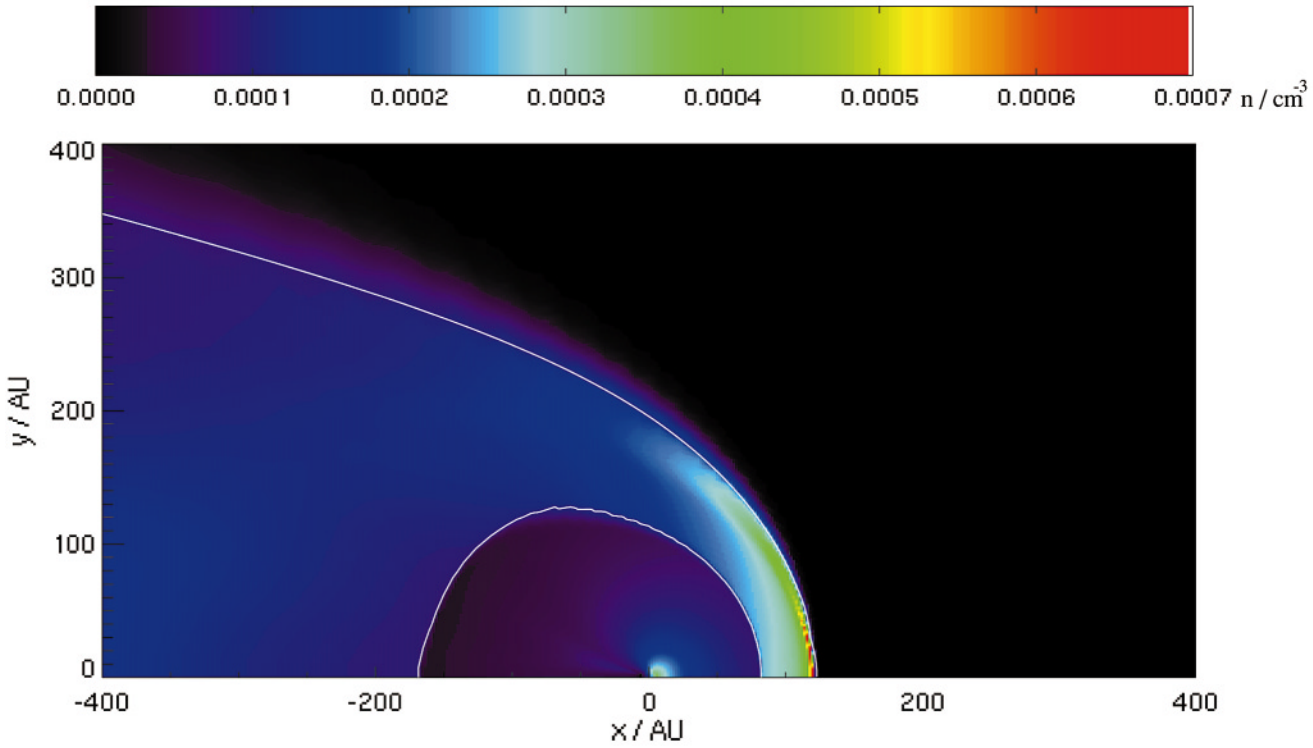

Fig. 12. Contour plot of the resulting pick-up ion density pattern. The position of the heliopause and solar wind termination shock is indicated by the white straight lines. The stream lines of the pick-up ions are equivalent to the solar wind proton stream lines (see Fig. 10). (Notice the different scaling of the x-axis in this figure and in Fig. 10). Outside the heliosphere pick-up ions do not exist. The part of pick-up ions outside the heliosphere shown in this figure is caused by the granularity of our numerical procedure using a grid with a finite resolution (Sect. 3).

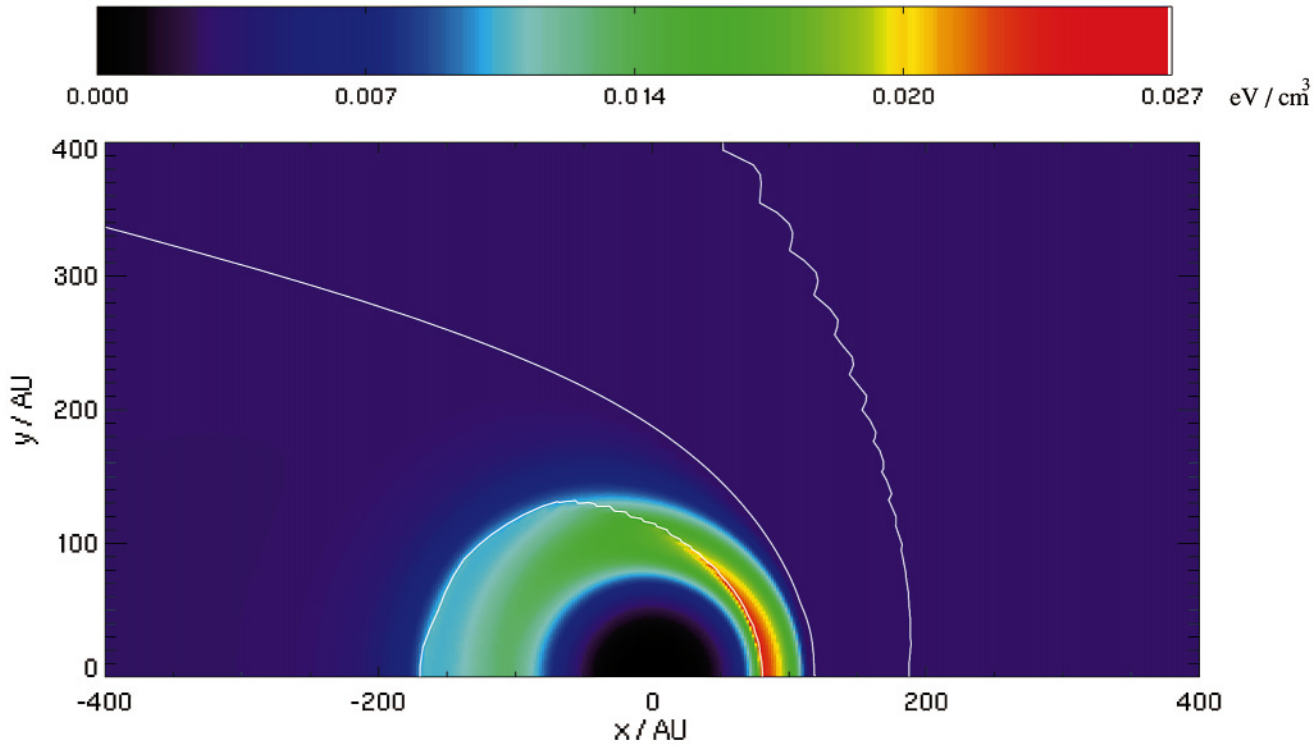

Fig. 13. Contour plot of the resulting ACR pressure pattern ([eV/cm^3]). Again the proton plasma bow-shock, the heliopause and the solar wind termination shock radius are shown as white straight lines (see Fig. 10). The structure seen in the position of the bow-shock is an artificial result of our numerical procedure using a finite grid method (Sect. 3) and the used graphic software.

work would for the first time allow to describe the consistent 3-d propagation of ACR‘s and GCR‘s on the basis of a multifluid plasma interface. Not only the tensorial character of the spatial diffusion could be explicitly taken into account, but in addition the ACR and GCR drift motions which are shown to be fairly important for the phase-space propagation of energetic particles (see Jokipii, 1992a) could quantitatively be taken into account. We are planning to go this way of modelling in the near future.

Acknowledgements. The authors are very grateful for financial support granted by the Deutsche Forschungsgemeinschaft in the frame of project Fa 97/23-2.

References

Axford W.I., Ip W.H., 1986, Adv. Space Res. 6(2), 27
Baranov V.B., Malama Y., 1993, JGR 103, 15157
Baranov V.B., Krasnobaev K.V., Ruderman M.S., 1976, Ap&SS 41, 481
Bertaux J.L., Lallement R., Kurt V.G., Mironova E.N., 1985, A&A 150, 1
Chalov S.V., Fahr H.J., 1994, A&A 288, 973
Chalov S.V., Fahr H.J., 1995, Space Sci. Rev. 72, 237
Chalov S.V., Fahr H.J., 1997, A&A 326, 860
Czechowski A., Grzedzielski S., Mostafa I., 1995, A&A 297, 892
Czechowski A., Fahr H.J., Fichtner H., Kausch T., 1999, 26th International Cosmic Ray Conference, Salt Lake City, Utah, August 17–25, 1999, Vol. 7, SH 4.1.03, 464
Donohue D.J., Zank G.P., 1993, JGR 98, 19005
Dworsky A., Fahr H.J., 2000, A&A 353, L1
Fahr H.J., 1974, Space Sci. Rev. 15, 483
Fahr H.J., Lay G., 2000, A&A, in press
Fahr H.J., Fichtner H., 1995, Solar Phys. 158, no. 2, 353
Fahr H.J., Osterbart R., Rucinski D., 1993, A&A 274, 612
Fahr H.J., Fichtner H., Grzedzielski S., 1992, Solar Phys. 137, 355
Fichtner H., Fahr H.J., Sreenivasan S.R., 1993, Proc. 23rd Int. Cosm. Ray Conf., Calgary (Canada), Vol. 3, 423
Fichtner H., Fahr H.J., Grzedzielski S., Rucinski D., Sreenivasan S.R., 1994, A&A 284, 599
Fichtner H., Sreenivasan S.R., Fahr H.J., 1996, A&A 308, 248
Fisk L.A., Kozlovsky B., Ramaty R., 1974, ApJ 190, L35
Fisk L.A., 1976a, JGR 81, 4633
Fisk L.A., 1976b, JGR 81, 4641
Fisk L.A., 1976c, ApJ 206, 333
Fite W., Smith A., Stebbings R., 1962, Proc. R. Soc. London Ser. A 268, 527
Gloeckler G., Geiss J., 1998, Space Sci. Rev. 86, 127
Gloeckler G., Geiss J., Balsiger H., et al., 1993, Sci 261, 70
Grzedzielski S., Fahr H.J., Fichtner H., 1992, In: Marsch E., Schwenn R. (eds.) Solar Wind VII, Proc. 3rd COSPAR-Coll., Goslar (Germany), Pergamon Press, p. 173
Izmodenov V., 1997, Adv. Space Res. 19, 965
Jokipii J.R., 1990, Physics of the outer heliosphere. Proceedings of the 1st COSPAR Coll. Warsaw, Poland,Sept. 19–22, 1989, (A91-55051 24-90), Oxford, England and Elmsford, NY, Pergamon Press, p. 169
Jokipii J.R., 1992a, In: Particle accelleration in cosmic plasmas. Proceedings of the Workschop, Bartol Research Inst., Newark, DE, Dec. 4–6,1991, (A 93-39976 16-93), p. 137
Jokipii J.R., 1992b, ApJ 393, L41
Kausch T., 1998, Ph.D. Thesis, Institut für Astronomie und Extraterrestrische Forschung der Universität Bonn
Kausch T., Fahr H.J., 1997, A&A 325, 828
Kota J., Jokipii J.R., 1993, Adv. Space Res. 13, 257
Lee M.A., Shapiro V.D., Sagdeev R.Z., 1996, JGR 101, 4777
Le Roux J.A., Fichtner H., 1997, JGR 102, 17365
Le Roux J.A., Potgieter M.S., 1993, Adv. Space Res. 13, 251
Liewer P.C., Rath S., Goldstein B.E., 1995, JGR 100, 19898
Linde T.J., Gombosi T.I., Ror P.L., Powell K.G., DeZeeuw D.L., 1998, JGR 103, 1889
McNutt R.L., Lyon J., Goodrich C.C., 1998, JGR 103, 1905
McNutt R.L., Lyon J., Goodrich C.C., Wildberg M., 1999, Solar Wind Nine. CP471, 823
Möbius, 1996, Space Sci. Rev. 78, 375
Myasnikov A., Izmodenov V., Chalov S., Aleksashov D., 1997, On the influence of galactic cosmic rays on the structure of heliospheric interface. Preprint No. 597, Institute for Problems in Mechanics, Moscow
Osterbart R., Fahr H.J., 1992, A&A 264, 260
Palmer I.D., 1982, Rev. Geophys. and Space Phys. 20, 335
Parker E.N., 1963, Interplanetary Dynamical Processes. John Wiley and Sons, New York
Pauls H., Zank G.P., 1996, JGR 101(A8), 17081
Pauls H., Zank G.P., 1995
Pogorelov N., Matsuda T., 1998, JGR 10, 237
Pogorelov N., Matsuda T., 2000, A&A 354, 697
Ptuskin V.S, 1981, Ap&SS 76, 265
Ratkiewicz R., Barnes A., Molvik G.A., et al., 1998, A&A 335, 363
Rice W.K.M., Zank G.P., 1999, 26th International Cosmic Ray Conference, Salt Lake City, Utah, August 17–25, 1999, SH 2.3.11
Roe P.L., 1981, J. of Comp. Phys. 43, 357
Steinolfson R.S., Pizzo V.J., Holzer T., 1994, Geophys. Res. Lett. 21, 245
Witte M., Rosenbauer H., Banaszkiewicz M., Fahr H.J., 1993, Adv. Space Res. 13 (6), 121
Zank G.P., 1999, Space Sci. Rev. 89, 413
Zank G.P., Webb G.M., Donohue D.J., 1993, ApJ 406, 67
Zank G.P., Pauls H.L., William L.L., Hyll D.T., 1996a, JGR 101, 21,639
Zank G.P., Pauls H.L., Cairns I.H., Webb G.M., 1996b, JGR 101, 457